

000  
001  
002054  
055  
056003  
004  
005  
006  
007057  
058  
059  
060  
061008  
009  
010  
011  
012062  
063  
064  
065  
066013  
014  
015067  
068  
069016  
017  
018  
019  
020070  
071  
072  
073  
074021  
022  
023  
024  
025075  
076  
077  
078  
079026  
027  
028  
029  
030080  
081  
082  
083  
084031  
032  
033  
034  
035  
036  
037  
038  
039  
040  
041  
042  
043  
044  
045  
046  
047  
048  
049  
050  
051  
052  
053085  
086  
087  
088  
089  
090  
091  
092  
093  
094  
095  
096  
097  
098  
099  
100  
101  
102  
103  
104  
105  
106  
107

# External Patch Group Prior Guided Internal Subspace Learning for Real Image Denoising

Anonymous CVPR submission

Paper ID \*\*\*\*

## Abstract

Existing image denoising methods largely depends on noise modeling and estimation. The commonly used noise models, additive white Gaussian, are inflexible in describing the complex noise on real noisy images. This would limit the performance of existing methods on denoising real noisy images. In this paper, we firstly demonstrate that almost all state-of-the-art methods on removing Gaussian noise and real noise are limited in denoising real noisy images. We demonstrate that a simple Patch Group based Prior Learning model on RGB images can achieve better performance than existing denoising methods, especially the ones designed for real noise in natural images. Besides, we employ the external patch group prior learning for internal clustering and subspace learning. This external information guided internal denoising methods achieves even better than the external PG prior based methods and the fully internal PG prior based method. Through extensive on standard datasets on real noisy images with groundtruth, we demonstrate that the proposed method achieves much better denoising performance than the other state-of-the-art methods on Gaussian noise removal and real noise removal.

## 1. Introduction

Image denoising is a fundamental problem in computer vision and image processing. It is an ideal platform for testing natural image models and provides high-quality images for other computer vision tasks such as image registration, segmentation, and pattern recognition, etc. For several decades, there emerge numerous image denoising methods [1, 2, 3, 4, 5, 6, 7, 8, 9, 10, 11], and all of them focus mainly on dealing with additive white Gaussian noise (AWGN). However, the images captured by CMOS or CCD cameras will undertake an in-camera imaging pipeline. The in-camera imaging pipeline includes mainly image demosaicing, white balance and color space transform, gamut mapping, tone mapping, and JPEG compression [12, 13].

Therefore, the noise in real images are much more complex than Gaussian, and depends on camera series, brands, as well as the settings (ISO, shutter speed, and aperture, etc). The models designed to deal with AWGN would become much less effective on real noisy images.

In the last decade, the methods of [14, 15, 16, 17, 18, 19, 13] are designed to deal with real noisy images. Almost all these methods coincidentally employ a two-stage framework: in the first stage, assuming a distribution model (usually Gaussian) on the noise and estimate its parameters; in the second stage, performing denoising with the help of the noise modeling and estimation in the first stage. However, the Gaussian assumption is inflexible in describing the complex noise on real noisy images [16]. Although the mixture of Gaussians (MoG) model is possible to approximate any unknown noise [19], estimating its parameters is often time consuming via nonparametric Bayesian techniques [19, 20]. To evaluate the performance of these methods on dealing with complex real noise, we apply these methods, with corresponding default parameters, on a real noisy image provided in [13]. This image is captured by a Nikon D800 camera while the ISO is set as 3200. The "ground truth" image is also provided with which we can calculate objective measurements. More details about this dataset can be found at the experimental section. The denoised images are listed in Figure 1, from which we can see that these methods either remove the noise or oversmooth the complex details in real noisy image. This proves that the above mentioned methods are not effective on denoising complex noise on real images.

In this paper, we attempt to deal with complex noise in real images by integrating the external and internal information. Since the real noise is signal dependent [13, 23], the prior information in external natural images can be employed to avoid the high correlation between noise and signal in internal images. On the other hand, the internal prior is adaptive to the image and can recover better the latent clean image. Based on these observations, we make detailed study on internal and external information for real image denoising task. We made several observa-

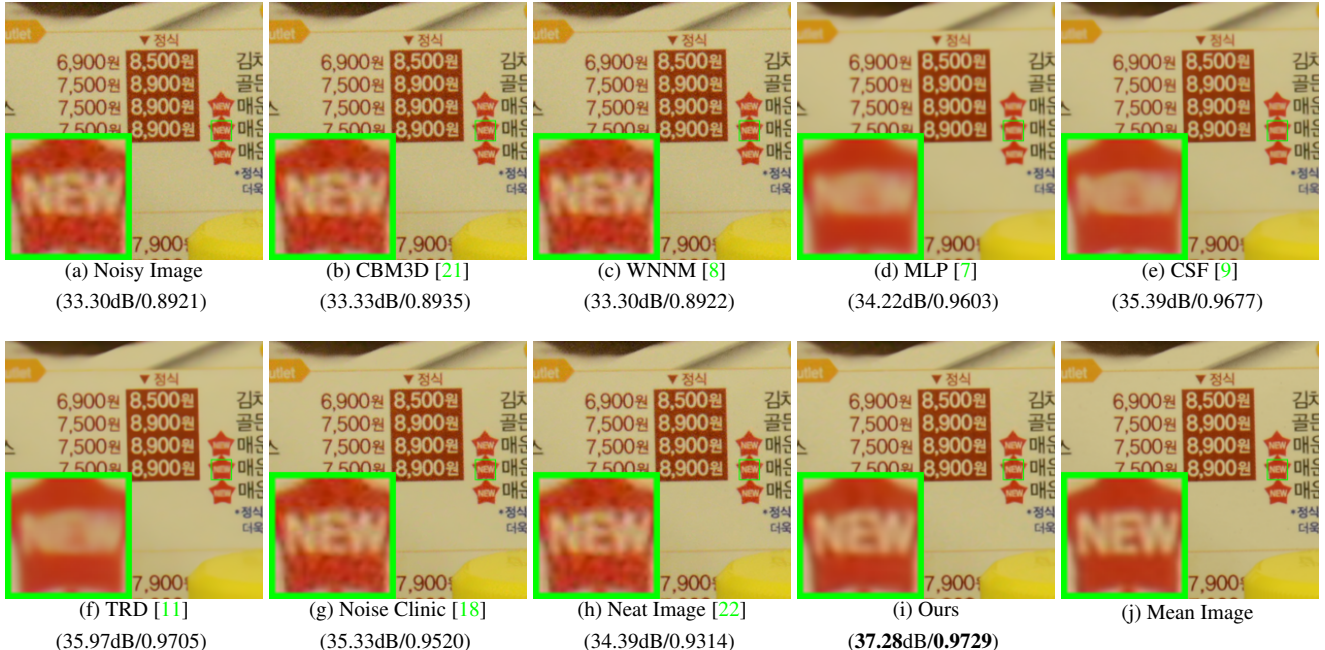


Figure 1. Denoised images of the real noisy image “*Nikon D800 ISO3200 A3*” by different methods. The images are better to be zoomed on screen.

tions. Firstly, we found that the Patch Group Prior learning based denoising method [10] learned on clean RGB images are enough to outperform the above mentioned denoising methods. Secondly, we also found that a fully internal PG prior based denoising method which achieve better performance than the fully external method. Most importantly, we found that the external PG prior guided internal method can achieve even better and faster performance on real image denoising. In fact, the external PG prior learning based model is employed to guide the clustering of internal PGs extracted from the input noisy images. Then for each cluster of PGs, we perform subspace learning by PCA and denoising by weighted sparse coding. We perform comprehensive experiments on real noisy images captured by different CMOS or CCS sensors. The results demonstrate that our method achieves comparable or even better performance on denoising real noisy images. An initial glimpse of our method is also listed in Figure 1. This reveals the potential advantages of combining external and internal information of natural images on robust and complex real noisy image denoising problem.

## 1.1. Our Contributions

The contributions of this paper are summarized as follows:

- We propose a novel method which combine the external and internal PG prior for real noisy image denoising problem;

- Our method doesn’t need noise modeling and estimation, and the noise levels of real noisy images are automatically expressed by the singular values of learned subspace;
- We achieve much better performance on visual quality, PSNR, SSIM, and speed, than other competing methods for real image denoising problem.

The rest of this paper will be summarized as follows: in Section 2, we will introduce the related work close to our work; in Section 3, we will introduce our proposed external prior guided internal subspace learning framework for real image denoising; in Section 4, we will demonstrate the denoising experiments on several standard dataset; in Section 5, we will conclude our paper and give our future work.

## 2. Related Work

### 2.1. Patch Group Prior of Natural Images

The Patch Group (PG) prior [10] is proposed to directly model the non-local self similar (NSS) property of natural images. The NSS property is commonly used in image restoration tasks [1, 4, 5, 8, 10]. The PG prior largely reduces the space of images to be modeled when compared to the patch prior [6]. The better modeling on NSS is demonstrated via better image denoising performance on natural images. However, in [10], only the PGs of clean natural images is utilized, while the PGs of noisy input images are ignored. In this paper, we aim at making use of both PGs

216 from natural clean images and real noisy images for better  
217 denoising performance.  
218

## 219 2.2. Internal v.s. External Image Denoising 220

221 For natural images, the internal patch recurrence across  
222 multiple scales has been successfully applied in many  
223 image restoration problems [24, 25, 26, 27]. These  
224 work demonstrate that internal information is enough for  
225 many ill-posed problems including denoising additive white  
226 Gaussian noise. The rationale is, since the AWGN noise is  
227 independent of the original clean images, it will be reduced  
228 if the image is scaled to a smaller size. However, the noise  
229 in real images is generated mostly from the camera sensors,  
230 which is highly complex and signal dependent [13]. Be-  
231 sides, according to the seminar workd of [23], the noise in  
232 real images has fixed patterns from several main sources.  
233 Therefore, we can hardly seperate the complex noise from  
234 the signals without the help of external (correct) informa-  
235 tion of natural clean images. Only using the internal infor-  
236 mation may be not enough for real image denoising prob-  
237 lem. On the other hand, the methods only using the exter-  
238 nal information may be not adaptive for real noisy images.  
239 Recently, the methods of [7, 9, 11] had been proposed to  
240 learn, on both internal and external images, a process di-  
241 rectly mapping the noisy patches to denoised ones. These  
242 discriminative learning based methods are only effective on  
243 additive white Gaussian noise and ineffective on complex  
244 and signal dependent noise in real images. This has been  
245 shown in Figure 1. In this paper, wour goal is to make use  
246 of external information to guide the subspace learning of  
247 internal PGs for image denoising task.  
248

## 249 2.3. Real Image Denoising

250 To the best of our knowledge, the study of real image  
251 denoising can be dated back to the BLS-GSM model [28],  
252 in which Portilla et al. proposed to use scale mixture of  
253 Gaussian in overcomplete oriented pyramids to estimate the  
254 latent clean images. In [14], Portilla proposed to use a cor-  
255 related Gaussian model for noise estimation of each wavelet  
256 subband. Based on the robust statistics theory [?], the work  
257 of Rabie [15] modeled the noisy pixels as outliers, which  
258 could be removed via Lorentzian robust estimator. In [16],  
259 Liu et al. proposed to use 'noise level function' (NLF) to es-  
260 timate the noise and then use Gaussian conditional random  
261 field to obtain the latent clean image. Recently, Gong et al.  
262 proposed an optimization based method [17], which mod-  
263 els the data fitting term by weighted sum of  $\ell_1$  and  $\ell_2$  norms  
264 and the regularization term by sparsity prior in the wavelet  
265 transform domain. Later, Lebrun el al. proposed a multi-  
266 scale denoising algorithm called 'Noise Clinic' [18] for  
267 real image denoising task. This method generalizes the NL-  
268 Bayes [29] to deal with signal, scale, and frequency depen-  
269 dent noise. Recently, Zhu et al. proposed a Bayesian model

270 [19] which approximates the noise via Mixture of Gaussian  
271 (MoG) model [20]. The clean image is recovered from the  
272 noisy image by the proposed Low Rank MoG filter (LR-  
273 MoG). However, noise level estimation is already a chal-  
274 lenging problem and denoising methods are quite sensitive  
275 to this parameter. Moreover, these methods are based on  
276 shrinkage models that are too simple to reflect reality, which  
277 results in over-smoothing of important structures such as  
278 small-scale text and textures.  
279

## 280 3. External Patch Group Prior Guided Inter- 281     nal Subspace Learning

282 In this section, we formulate the framework of external  
283 Patch Group prior guided internal subspace learning. We  
284 first introduce the patch group prior leaning on clean natural  
285 RGB images. Then we formulate the external guided inter-  
286 nal subspace learning. Finally, we discuss the differences  
287 between external subspaces and the corresponding internal  
288 subspace.  
289

### 290 3.1. External Patch Group Prior Learning

291 Natural images often demonstrate repetitive patterns,  
292 this nonlocal self-similarity (NSS) property is a key suc-  
293 cessful factor for many image denoising methods [1, 4, 5,  
294 30, 8, 10] and restoration methods [ ]. In [10], the NSS prop-  
295 erty is directly learned as an external prior in a patch group  
296 manner. In this section, we formulate the Patch Group prior  
297 on natural color images.  
298

299 In [10], the patch group (PG) is defined as a group of  
300 similar patches to the local patch. The patch group mean  
301 is destracted, and hence different groups patches can share  
302 similar PGs. Therefore the space to be modeled is largely  
303 reduced. In this work, we extract PGs from RGB im-  
304 ages. Each patch is of size  $p \times p \times 3$ . For each local  
305 patch, we search its similar patches around it through the  
306 Euclidean distance in a local window of size  $W \times W$ .  
307 The PG is denoted by  $\{\mathbf{x}_m\}_{m=1}^M$ , where  $\mathbf{x}_m \in \mathbb{R}^{3p^2 \times 1}$   
308 is a color image patch vector. The mean vector of this  
309 PG is  $\boldsymbol{\mu} = \frac{1}{M} \sum_{m=1}^M \mathbf{x}_m$ , and  $\bar{\mathbf{x}}_m = \mathbf{x}_m - \boldsymbol{\mu}$  is the  
310 group mean subtracted patch vector. The PG is defined as  
311  $\bar{\mathbf{X}} \triangleq \{\bar{\mathbf{x}}_m\}, m = 1, \dots, M$ , and it represent the external  
312 NSS prior on color images. Assume we have extracted  $N$   
313 PGs from a given set of natural images, and the  $n$ -th PG  
314 is defined as  $\bar{\mathbf{X}}_n \triangleq \{\bar{\mathbf{x}}_{n,m}\}_{m=1}^M, n = 1, \dots, N$ . We employ  
315 the patch group based Gaussian Mixture Model (PG-GMM)  
316 for NSS prior learning. We aim to learn a set of  $K$  Gaus-  
317 sians  $\{\mathcal{N}(\boldsymbol{\mu}_k, \Sigma_k)\}$  from  $N$  training PGs  $\{\bar{\mathbf{X}}_n\}$ , while  
318 requiring that all the  $M$  patches  $\{\bar{\mathbf{x}}_{n,m}\}$  in PG  $\bar{\mathbf{X}}_n$  belong to  
319 the same Gaussian component and assume that the patches  
320 in the PG are independently sampled. Note that such an as-  
321 sumption is commonly used in patch based image modeling  
322

324 [3, 5]. Then, the likelihood of  $\{\bar{\mathbf{X}}_n\}$  can be calculated as  
 325  
 326  
 327

$$P(\bar{\mathbf{X}}_n) = \sum_{k=1}^K \pi_k \prod_{m=1}^M \mathcal{N}(\bar{\mathbf{x}}_{n,m} | \boldsymbol{\mu}_k, \boldsymbol{\Sigma}_k). \quad (1)$$

328 By assuming that all the PGs are independently sampled,  
 329 the overall objective log-likelihood function is  
 330

$$\ln \mathcal{L} = \sum_{n=1}^N \ln \left( \sum_{k=1}^K \pi_k \prod_{m=1}^M \mathcal{N}(\bar{\mathbf{x}}_{n,m} | \boldsymbol{\mu}_k, \boldsymbol{\Sigma}_k) \right). \quad (2)$$

331 We maximize the above objective function for PG-GMM  
 332 learning and finally obtain the GMM model with learned  
 333 parameters including mixture weights  $\{\pi_k\}_{k=1}^K$ , mean vectors  
 334  $\{\boldsymbol{\mu}_k = \mathbf{0}\}_{k=1}^K$ , and covariance matrices  $\{\boldsymbol{\Sigma}_k\}_{k=1}^K$ . Noted  
 335 that the mean vector of each cluster is natural zeros, i.e.,  
 336  $\boldsymbol{\mu}_k = \mathbf{0}$ .  
 337

### 338 3.2. External Prior Guided Internal Subspace 339 Learning

340 Given a real noisy image, we extract noisy PGs from it  
 341 and save the mean vectors of each PG for recovering. The  
 342 mean subtracted PG is defined as  $\bar{\mathbf{Y}}$ . To project this PG  
 343 into a most adaptive subspace, we select the most suitable  
 344 Gaussian component to it from the PG-GMM trained in pre-  
 345 vious section. The selection can be done by checking the  
 346 posterior probability that  $\bar{\mathbf{Y}}$  belongs to the  $k$ th Gaussian  
 347 component:  
 348

$$P(k|\bar{\mathbf{Y}}) = \frac{\prod_{m=1}^M \mathcal{N}(\bar{\mathbf{y}}_m | \mathbf{0}, \boldsymbol{\Sigma}_k)}{\sum_{l=1}^K \prod_{m=1}^M \mathcal{N}(\bar{\mathbf{y}}_m | \mathbf{0}, \boldsymbol{\Sigma}_l)}. \quad (3)$$

349 Since the noise on real images are mostly small when com-  
 350 pared to the signals, the covariance matrix of the  $k$ th com-  
 351 ponent is still  $\boldsymbol{\Sigma}_k$ . Finally, the component with the maxi-  
 352 mum A-posteriori (MAP) probability  $\ln P(k|\bar{\mathbf{Y}})$  is selected  
 353 as the most suitable subspace for  $\bar{\mathbf{Y}}$ .  
 354

355 Though each PG has been projected into its most suitable  
 356 subspace, the pre-learned subspace is still too general to  
 357 represent the noisy PG extracted from the real noisy image.  
 358 That is, the noisy PGs projected into one cluster can still  
 359 constisted a subspace which is of lower dimensions than the  
 360 subspace pre-learned from the external PGs. This can be  
 361 demonstrated by compare the distribution of external PGs  
 362 and internal PGs in the same clusters. We randomly select  
 363 one cluster, and collect the clean PGs extracted from exter-  
 364 nal dataset (Kodak 24 images) and the noisy PGs from the  
 365 testing image. Since the original PGs are of  $3p^2$  dimensions,  
 366 we apply PCA to project the PGs into 2 dimensions for bet-  
 367 ter visualization. The results is shown in Figure ??, from  
 368 which we can see clearly that the projected PGs are mainly  
 369 in a smaller region of the external PGs, which proves that  
 370 the internal PGs are only consisted a subspace in a lower  
 371 dimension than the PGs collected from external subspace.  
 372

373 To better and adaptively charactering the internal PGs from  
 374 the testing image, we need learn a more specific dictionary  
 375 for noisy PGs assigned into each cluster. For notation sim-  
 376 plicity, we ignore the index of subspace  $k$ . The internal PGs  
 377  $\mathbf{Y}$  form a subspace which can be obtained by singular value  
 378 decomposition (SVD),  
 379

$$\mathbf{Y} = \mathbf{U} \mathbf{S} \mathbf{V}^T \quad (4)$$

380 The singular vectors capture the statistical structures of NSS  
 381 variations in natural images, while the singular values in  $\mathbf{S}$   
 382 represent the significance of these singular vectors. Fig. 4  
 383 shows the singular vectors for one Gaussian component.  
 384

### 385 3.3. What does External Prior help the Internal 386 Subspace Learning?

387 Until now, we have divided the noisy PGs into multiple  
 388 internal subspaces. Here we take a deep analysis on how the  
 389 external NSS prior guide the subspace learning of internal  
 390 PGs. The help are at least threefold. Firstly, through MAP  
 391 in (3), the external prior guides the noisy PGs to be clustered  
 392 into the correct subspaces. If we cluster the noisy PGs in an  
 393 automatical way, the subspaces we learned will be highly  
 394 degraded by the signal dependent noise. Secondly, the guid-  
 395 ance of external prior for internal clustering is more efficient  
 396 than directly clustering the internal noisy PGs. It only needs  
 397 to calculate the MAP probability via the equation (3) while  
 398 the internal clustering via GMM is time-consuming on EM  
 399 algorithm [31]. Thirdly, due to the correct guidance of ex-  
 400 ternal prior, the structural decomposition via SVD of each  
 401 subspace is more adaptive. This will bring better denois-  
 402 ing performance than the methods only using the external  
 403 information.  
 404

### 405 3.4. Discussion on Internal Subspace Structure

406 The Internal PGs are in fact lying in the subspaces of  
 407 external PG Spaces. To defend this argument, we com-  
 408 pare the distribution of external PGs extracted from clean  
 409 natural images and real noisy images. For better illumina-  
 410 tion, we randomly selected a cluster and project the orig-  
 411 inal clean PGs  $\mathbf{X}$  onto a 2-D plane. This could be done  
 412 via  $\mathbf{X}_p = \mathbf{U}(:, 1 : 2)^T \mathbf{X}$ , where  $\mathbf{U}$  is the singular vector  
 413 matrix of that cluster. The noisy PGs  $\mathbf{Y}$  assigned in this  
 414 cluster is also projected into 2-D via  $\mathbf{Y}_p = \mathbf{U}(:, 1 : 2)^T \mathbf{Y}$ .  
 415 The Figure ?? reflects the distribution on the 2-D plane of  
 416 the projected clean PGs from external natural images and  
 417 the projected noisy PGs from internal image. We can see  
 418 that the internal noisy PGs are indeed lying in a subspace  
 419 of the external PGs. Hence, if we directly use the external  
 420 prior learned from clean PGs, the learned subspaces would  
 421 be too generative to be suitable for the testing data.  
 422

423 Through SVD, the PGs in each internal subspace can be  
 424 divided into singular vectors and singular values. The sin-  
 425 gular vectors are the basis of the corresponding subspace  
 426

427  
 428  
 429  
 430  
 431

432 while the singular values reflect the importance of these basis.  
 433 The basis can be used as dictionary to code the noisy  
 434 PGs. And the singular values are adaptive parameters for  
 435 internal noisy PGs. We can compare the singular values of  
 436 one internal subspace and the corresponding space of ex-  
 437 ternal PGs. The result is shown in Figure ???. From which  
 438 we can see that the noisy subspace often have higher val-  
 439 ues than external space consisted of clean PGs. This gap is  
 440 clearly made of the noise and can be used for image denois-  
 441 ing in a natural way.  
 442

## 4. The Denoising Algorithm

445 We employ the  $\mathbf{U}$  as the adaptive dictioanry to represent  
 446 the structural variations of the PGs in that component.  
 447

$$\min_{\alpha} \|\bar{\mathbf{y}}_m - \mathbf{U}\alpha\|_2^2 + \sum_{i=1}^{3p^2} \lambda_i |\alpha_i|. \quad (5)$$

451 The  $i$ th entry of the regularization parameter  $\lambda_i$   
 452

$$\lambda_i = \frac{\lambda}{\mathbf{S}_i + \varepsilon}, \quad (6)$$

453 where  $\varepsilon$  is a small positive number to avoid dividing by zero.  
 454 Since the dictionary  $\mathbf{U}$  is orthonormal, it is not difficult to  
 455 find out that (4) has a closed-form solution (detailed deriva-  
 456 tion can be found in the supplementary material):  
 457

$$\hat{\alpha} = \text{sgn}(\mathbf{U}^T \bar{\mathbf{y}}_m) \odot \max(|\mathbf{U}^T \bar{\mathbf{y}}_m| - \Lambda, \mathbf{0}), \quad (7)$$

458 where  $\Lambda = [\lambda_1, \lambda_2, \dots, \lambda_{3p^2}]$  is the vector of regulariza-  
 459 tion parameter and  $\text{sgn}(\bullet)$  is the sign function,  $\odot$  means  
 460 element-wise multiplication, and  $|\mathbf{U}^T \bar{\mathbf{y}}_m|$  is the absolute  
 461 value of each entry of vector  $|\mathbf{U}^T \bar{\mathbf{y}}_m|$ . The closed-form  
 462 solution makes our weighted sparse coding process very  
 463 efficient.  
 464

### 4.1. Iterative Regularization

470 Perfoming image denoising in one iteration is not  
 471 enough for real noise since the noise is signal dependent.  
 472 The removed noise in one iteration is largely dependent on  
 473 the signal. Therefore, it is essential to add back some resi-  
 474 duals removed in this iteration for the denoising of the next  
 475 iteration.  
 476

### 4.2. Effectively dealing with different noisy images

478 For real image denoising, we can perform well on images  
 479 which have similar noise levels with the training dataset.  
 480 How can we deal with the real noisy images whose noise  
 481 levels are higher than the training dataset? The answer is  
 482 to remove the noise by more iterations. The input image of  
 483 each iteration is the recovered image of previous iteration.  
 484 This makes sense since we can still view the recovered im-  
 485 age as a real noisy image.  
 486

---

### Alg. 1: External Guided Internal Subspace Denoising

---

Input: Noisy image  $\mathbf{y}$ , PG-GMM model

1. Initialization:  $\hat{\mathbf{x}}^{(0)} = \mathbf{y}, \mathbf{y}^{(0)} = \mathbf{y};$

for  $t = 1 : IteNum$  do

2. Iterative Regularization:

$$\mathbf{y}^{(t)} = \hat{\mathbf{x}}^{(t-1)} + \delta(\mathbf{y} - \mathbf{y}^{(t-1)});$$

3. Estimate the standard deviation of noise;

for each PG  $\mathbf{Y}$  do

4. Calculate group mean  $\mu_y$  and form PG  $\bar{\mathbf{Y}}$ ;

5. Gaussian component selection via (3);

end for

for each Internal Subspace do

6. Internal Subspace Learning by (4);

7. Recover each patch in all PGs via  $\hat{\mathbf{x}}_m = \mathbf{D}\hat{\alpha} + \mu_y$ ;

end for

8. Aggregate the recovered PGs of all subspaces to form  
 the recovered image  $\hat{\mathbf{x}}^{(t)}$ ;

end for

Output: The recovered image  $\hat{\mathbf{x}}^{(IteNum)}$ .

---

This will also bring a second problem, that how we could automatically terminate the iteration. This can be solved by two methods. One way is to compare the images between two iterations and calculate their difference, the iteration can be terminated if the difference is smaller than a threshold. The other way is to estimate the noise level of the current image and terminate the iterations when the noise level is lower than a preset threshold. We employ the second way and set the threshold as 0.002 in our experiments. In fact, most of our testing images will be denoised well in one iteration.

### 4.3. The Overall Algorithm

With the solution  $\hat{\alpha}$  in (7), the clean patch in a PG can be estimated as  $\hat{\mathbf{x}}_m = \mathbf{D}\hat{\alpha} + \mu_y$ . Then the clean image  $\hat{\mathbf{x}}$  can be reconstructed by aggregating all the estimated PGs. In practice, we could perform the above denoising procedures for several iterations for better denoising outputs. In iteration  $t$ , we use the iterative regularization strategy [32] to add back to the recovered image  $\hat{\mathbf{x}}^{(t-1)}$  some estimation residual in iteration  $t-1$ . The proposed denoising algorithm is summarized in Algorithm 1 (Alg. 1).

## 5. Experiments

In this section, we perform real image denoising experiments on three standard datasets. The first dataset is real noisy images with mean images as ground truths provided by [13], some samples are shown in Figure 3. The second dataset is provided by the website of Noise Clinic [18]. The third dataset is provided by the Commercial software Neat Image [22]. The second and third dataset do not have ground truth images.



Figure 2. Some testing images in the dataset [13].



Figure 3. Some cropped images of the dataset [13].

## 5.1. Parameters Setting

The proposed method contains the PG prior learning stage, the external prior guided internal subspace learning stage, and the denoising stage. In the learning stage, similar to the PGPD, there are four parameters,  $p$ ,  $M$ ,  $W$ , and  $K$ . We set  $p = 6$  and hence the patch size is  $6 \times 6 \times 3$ . The window size for searching PGs is  $W = 31$ . The number of similar patches is  $N = 10$ , the number of clusters is set as  $K = 33$ . In the external prior guided learning stage, there is no parameters. In the denoising stage, there are one parameter, i.e., the  $\lambda$  which is used to regularize the sparse term.

## 5.2. Comparison on External and Internal methods

In this subsection, we compared the proposed external prior guided internal subspace learning model on real image denoising. The three methods are evaluated on the dataset provided in [13]. We calculate the PSNR, SSIM [?] and visual quality of these three methods. We also compare the speed. The PSNR and SSIM results on 60 cropped images from [13] are listed in Table 1. The images are cropped into size of  $500 \times 500$  for better illustration. We also compare the three methods on visual quality in Figure 5.2. Compare the denoised images listed in Figure 5.2 and Figure 5.2, we can see that the Offline method is better at edges, smooth regions while the Online method is good at complex textures. The reason is two folds. Firstly, the Offline method is learned on clean images and hence is better at representing edges, structures, and smooth area. The online method is influenced by the noise and hence some noise cannot be removed. Secondly, the Online method is better at recovering complex area since they could learn adaptive dictionaries for the specific area. The Offline method cannot recover the complex area since they did not learn the similar structures from the external natural clean images.

## 5.3. Comparison With other Competing Methods

We compare with previous state-of-the-art Gaussian noise removal methods such as BM3D [4], WNNM [8], MLP [7], CSF [9], and the recently proposed TRD [11]. We also compare with three competing real image denoising methods such as Noise Clinic, Neat Image, and the CCNoise method proposed recently. The popular software NeatImage which is one of the best denoising software available. All these methods need noise estimation which is very hard to perform if there is no uniform regions available in the testing image. The NeatImage will fail to perform automatical parameters settings if there is no uniform regions.<sup>1</sup>

We the competing denoising methods from various research directions on two datasets. Both the two datasets comes from the [13]. The first dataset contains 17 images of size over  $7000 \times 5000$ . Since this dataset contains recurrent contents across different images, we crop 60 small images of size  $500 \times 500$  from these 17 images in [13].

The PSNR and SSIM results are listed in table 2.

## 5.4. Discussion on Parameter $\lambda$

The proposed method only has a key parameter, namely the regularization parameter  $\lambda$ . To demonstrate that the proposed method is robust to the variance of  $\lambda$ , we vary the parameter  $\lambda$  across a wide range and obtain the PSNR and SSIM results as a function of the parameter  $\lambda$ . The results is shown in Figure 8, from which we can see that the proposed method can achieve a PSNR (SSIM) over 38.2dB (0.9620) when  $\lambda$  varies from  $1e-3$  to  $4e-4$ . This shows that the proposed method is indeed robust to the chosen of the parameter  $\lambda$ .

## 6. Conclusion and Future Work

In the future, we will evaluate the proposed method on other computer vision tasks such as single image super-resolution, photo-sketch synthesis, and cross-domain image recognition. Our proposed method can be improved if we use better training images, fine tune the parameters via cross-validation. We believe that our framework can be useful not just for real image denoising, but for image super-resolution, image cross-style synthesis, and recognition tasks. This will be our line of future work.

## References

- [1] A. Buades, B. Coll, and J. M. Morel. A non-local algorithm for image denoising. *CVPR*, pages 60–65, 2005. 1, 2, 3
- [2] S. Roth and M. J. Black. Fields of Experts. *International Journal of Computer Vision*, 82(2):205–229, 2009. 1

<sup>1</sup>To compare with CCNoise, we first transform the denoised images into double format.

648

649

650

651

652

653

654

655

656

657

658

659

660

661

662

663

664

665

666

667

668

669

670

671

672

673

674

675

676

677

678

679

680

681

682

683

684

685

686

687

688

689

690

691

692

693

694

695

696

697

698

699

700

701

702

703

704

705

706

707

708

709

710

711

712

713

714

715

716

717

718

719

720

721

722

723

724

725

726

727

728

729

730

731

732

733

734

735

736

737

738

739

740

741

742

743

744

745

746

747

748

749

750

751

752

753

754

755



Figure 4. Denoised images of the image "Nikon D600 ISO 3200 C1" by different methods. The images are better to be zoomed in on screen.

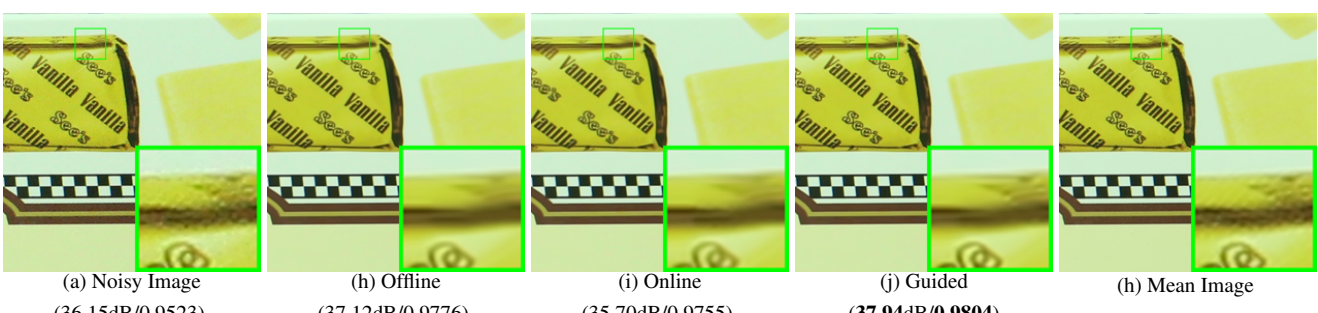


Figure 5. Denoised images of the image "Canon EOS 5D Mark3 ISO 3200 C1" by different methods. The images are better to be zoomed in on screen.

- [3] M. Elad and M. Aharon. Image denoising via sparse and redundant representations over learned dictionaries. *Image Processing, IEEE Transactions on*, 15(12):3736–3745, 2006. [1](#), [2](#), [3](#)
- [4] K. Dabov, A. Foi, V. Katkovnik, and K. Egiazarian. Image denoising by sparse 3-D transform-domain collaborative filtering. *Image Processing, IEEE Transactions on*, 16(8):2080–2095, 2007. [1](#), [2](#), [3](#), [6](#)
- [5] J. Mairal, F. Bach, J. Ponce, G. Sapiro, and A. Zisserman. Non-local sparse models for image restoration. *ICCV*, pages 2272–2279, 2009. [1](#), [2](#), [3](#), [4](#)
- [6] D. Zoran and Y. Weiss. From learning models of natural image patches to whole image restoration. *ICCV*, pages 479–486, 2011. [1](#), [2](#)
- [7] Harold C Burger, Christian J Schuler, and Stefan Harmeling. Image denoising: Can plain neural networks compete with bm3d? *Computer Vision and Pattern Recognition (CVPR), 2012 IEEE Conference on*, pages 2392–2399, 2012. [1](#), [2](#), [3](#), [6](#)
- [8] S. Gu, L. Zhang, W. Zuo, and X. Feng. Weighted nuclear norm minimization with application to image denoising. *CVPR*, pages 2862–2869, 2014. [1](#), [2](#), [3](#), [6](#)
- [9] U. Schmidt and S. Roth. Shrinkage fields for effective image restoration. *Computer Vision and Pattern Recognition (CVPR), 2014 IEEE Conference on*, pages 2774–2781, June 2014. [1](#), [2](#), [3](#), [6](#)
- [10] J. Xu, L. Zhang, W. Zuo, D. Zhang, and X. Feng. Patch group based nonlocal self-similarity prior learning for image

denoising. *2015 IEEE International Conference on Computer Vision (ICCV)*, pages 244–252, 2015. [1](#), [2](#), [3](#)

- [11] Yunjin Chen, Wei Yu, and Thomas Pock. On learning optimized reaction diffusion processes for effective image restoration. *Proceedings of the IEEE Conference on Computer Vision and Pattern Recognition*, pages 5261–5269, 2015. [1](#), [2](#), [3](#), [6](#)

- [12] S. J. Kim, H. T. Lin, Z. Lu, S. Ssstrunk, S. Lin, and M. S. Brown. A new in-camera imaging model for color computer vision and its application. *IEEE Transactions on Pattern Analysis and Machine Intelligence*, 34(12):2289–2302, Dec 2012. [1](#)

- [13] Seonghyeon Nam, Youngbae Hwang, Yasuyuki Matsushita, and Seon Joo Kim. A holistic approach to cross-channel image noise modeling and its application to image denoising. *Proc. Computer Vision and Pattern Recognition (CVPR)*, pages 1683–1691, 2016. [1](#), [3](#), [5](#), [6](#), [8](#)

- [14] J. Portilla. Full blind denoising through noise covariance estimation using gaussian scale mixtures in the wavelet domain. *Image Processing, 2004. ICIP '04. 2004 International Conference on*, 2:1217–1220, 2004. [1](#), [3](#)

- [15] Tamer Rabie. Robust estimation approach for blind denoising. *Image Processing, IEEE Transactions on*, 14(11):1755–1765, 2005. [1](#), [3](#)

- [16] C. Liu, R. Szeliski, S. Bing Kang, C. L. Zitnick, and W. T. Freeman. Automatic estimation and removal of noise from a single image. *IEEE Transactions on Pattern Analysis and Machine Intelligence*, 30(2):299–314, 2008. [1](#), [3](#)

756 Table 1. Average PSNR(dB) results of different methods on 60 cropped real noisy images captured in [13].  
757

	Noisy	CBM3D	WNNM	MLP	CSF	TRD	NI	NC	Offline	Online	Guided
PSNR	34.51	34.58	34.52	36.19	37.40	37.75	36.53	37.57	38.19	38.07	<b>38.55</b>
SSIM	0.8718	0.8748	0.8743	0.9470	0.9598	0.9617	0.9241	0.9514	0.9663	0.9625	<b>0.9675</b>

761 Table 2. Average PSNR(dB) results of different methods on 15 cropped real noisy images used in [13].  
762

Camera Settings	Noisy	CBM3D	WNNM	MLP	CSF	TRD	NI	NC	CC	Guided
Canon 5D Mark III ISO = 3200	37.00	37.08	37.09	33.92	35.68	36.20	37.68	38.76	38.37	<b>40.41</b>
	33.88	33.94	33.93	33.24	34.03	34.35	34.87	35.69	35.37	<b>37.14</b>
	33.83	33.88	33.90	32.37	32.63	33.10	34.77	35.54	34.91	<b>37.11</b>
Nikon D600 ISO = 3200	33.28	33.33	33.34	31.93	31.78	32.28	34.12	<b>35.57</b>	34.98	35.25
	33.77	33.85	33.79	34.15	35.16	35.34	35.36	<b>36.70</b>	35.95	36.60
	34.93	35.02	34.95	37.89	39.98	40.51	38.68	39.28	<b>41.15</b>	38.78
Nikon D800 ISO = 1600	35.47	35.54	35.57	33.77	34.84	35.09	37.34	38.01	37.99	<b>38.59</b>
	35.71	35.79	35.77	35.89	38.42	38.65	38.57	39.05	40.36	<b>40.44</b>
	34.81	34.92	34.95	34.25	35.79	35.85	37.87	38.20	38.30	<b>38.85</b>
Nikon D800 ISO = 3200	33.26	33.34	33.31	37.42	38.36	38.56	36.95	38.07	<b>39.01</b>	38.34
	32.89	32.95	32.96	34.88	35.53	35.76	35.09	35.72	<b>36.75</b>	<b>36.74</b>
	32.91	32.98	32.96	38.54	40.05	<b>40.59</b>	36.91	36.76	39.06	38.29
Nikon D800 ISO = 6400	29.63	29.66	29.71	33.59	34.08	34.25	31.28	33.49	<b>34.61</b>	33.37
	29.97	30.01	29.98	31.55	32.13	32.38	31.38	32.79	<b>33.21</b>	<b>33.21</b>
	29.87	29.90	29.95	31.42	31.52	31.76	31.40	32.86	33.22	<b>33.27</b>
Average PSNR	33.41	33.48	33.48	34.32	35.33	35.65	35.49	36.43	36.88	<b>37.09</b>
Average SSIM	0.8483	0.8511	0.8512	0.9113	0.9250	0.9280	0.9126	0.9364	0.9481	<b>0.9502</b>

782 [17] Zheng Gong, Zuowei Shen, and Kim-Chuan Toh. Image  
783 restoration with mixed or unknown noises. *Multiscale Mod-  
784*  
785  
786  
787788 [18] M. Lebrun, M. Colom, and J.-M. Morel. Multiscale image  
789 blind denoising. *Image Processing, IEEE Transactions on*,  
790 24(10):3149–3161, 2015. **1, 2, 3, 5**791 [19] Fengyuan Zhu, Guangyong Chen, and Pheng-Ann Heng.  
792 From noise modeling to blind image denoising. *The IEEE  
793 Conference on Computer Vision and Pattern Recognition  
794 (CVPR)*, June 2016. **1, 3**795 [20] C. M. Bishop. *Pattern recognition and machine learning*.  
796 New York: Springer, 2006. **1, 3**797 [21] K. Dabov, A. Foi, V. Katkovnik, and K. Egiazarian. Color  
798 image denoising via sparse 3d collaborative filtering with  
799 grouping constraint in luminance-chrominance space. *IEEE  
800 International Conference on Image Processing*, 1, 2007. **2**801 [22] Neatlab ABSoft. Neat image. [https://ni.  
802 neatvideo.com/home](https://ni.neatvideo.com/home). **2, 5**803 [23] Glenn E Healey and Raghava Kondepudy. Radiometric ccd  
804 camera calibration and noise estimation. *IEEE Transactions  
805 on Pattern Analysis and Machine Intelligence*, 16(3):267–  
806 276, 1994. **1, 3**807 [24] Daniel Glasner, Shai Bagon, and Michal Irani. Super-  
808 resolution from a single image. *ICCV*, 2009. **3**809 [25] Maria Zontak, Inbar Mosseli, and Michal Irani. Separating  
810 signal from noise using patch recurrence across scales. *Pro-  
811 ceedings of the IEEE Conference on Computer Vision and  
812 Pattern Recognition*, pages 1195–1202, 2013. **3**813 [26] Tomer Michaeli and Michal Irani. Blind deblurring using in-  
814 ternal patch recurrence. *European Conference on Computer  
815 Vision*, pages 783–798, 2014. **3**816 [27] Y. Bahat and M. Irani. Blind dehazing using internal patch  
817 recurrence. *IEEE International Conference on Computa-  
818 tional Photography (ICCP)*, pages 1–9, May 2016. **3**819 [28] J. Portilla, V. Strela, M.J. Wainwright, and E.P. Simoncelli.  
820 Image denoising using scale mixtures of Gaussians in the  
821 wavelet domain. *Image Processing, IEEE Transactions on*,  
822 12(11):1338–1351, 2003. **3**823 [29] M. Lebrun, A. Buades, and J. M. Morel. A nonlocal bayesian  
824 image denoising algorithm. *SIAM Journal on Imaging Sci-  
825 ences*, 6(3):1665–1688, 2013. **3**826 [30] W. Dong, L. Zhang, G. Shi, and X. Li. Nonlocally central-  
827 ized sparse representation for image restoration. *Image Pro-  
828 cessing, IEEE Transactions on*, 22(4):1620–1630, 2013. **3**829 [31] A. P. Dempster, N. M. Laird, and D. B. Rubin. Maximum  
830 likelihood from incomplete data via the EM algorithm. *Jour-  
831 nal of the Royal Statistical Society. Series B (methodologi-  
832 cal)*, pages 1–38, 1977. **4**833 [32] S. Osher, M. Burger, D. Goldfarb, J. Xu, and W. Yin. An it-  
834 erative regularization method for total variation-based image  
835

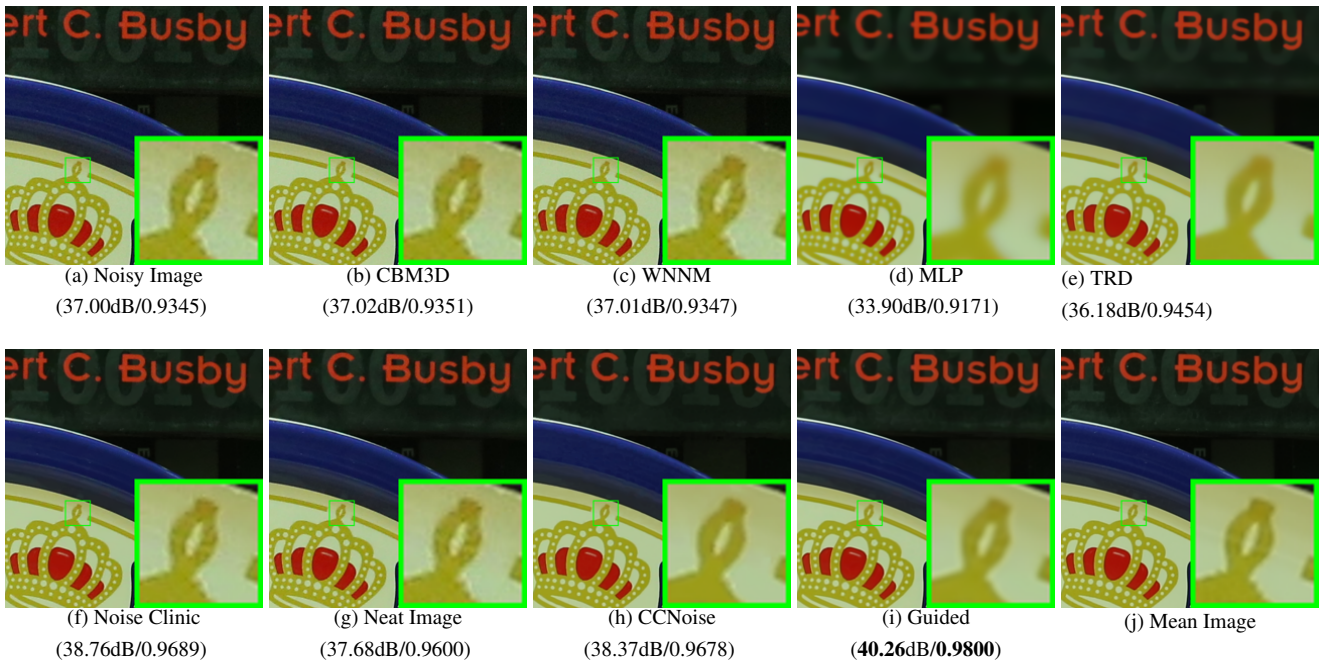


Figure 6. Denoised images of the image "Canon 5D Mark 3 ISO 3200 1" by different methods. The images are better to be zoomed in on screen.

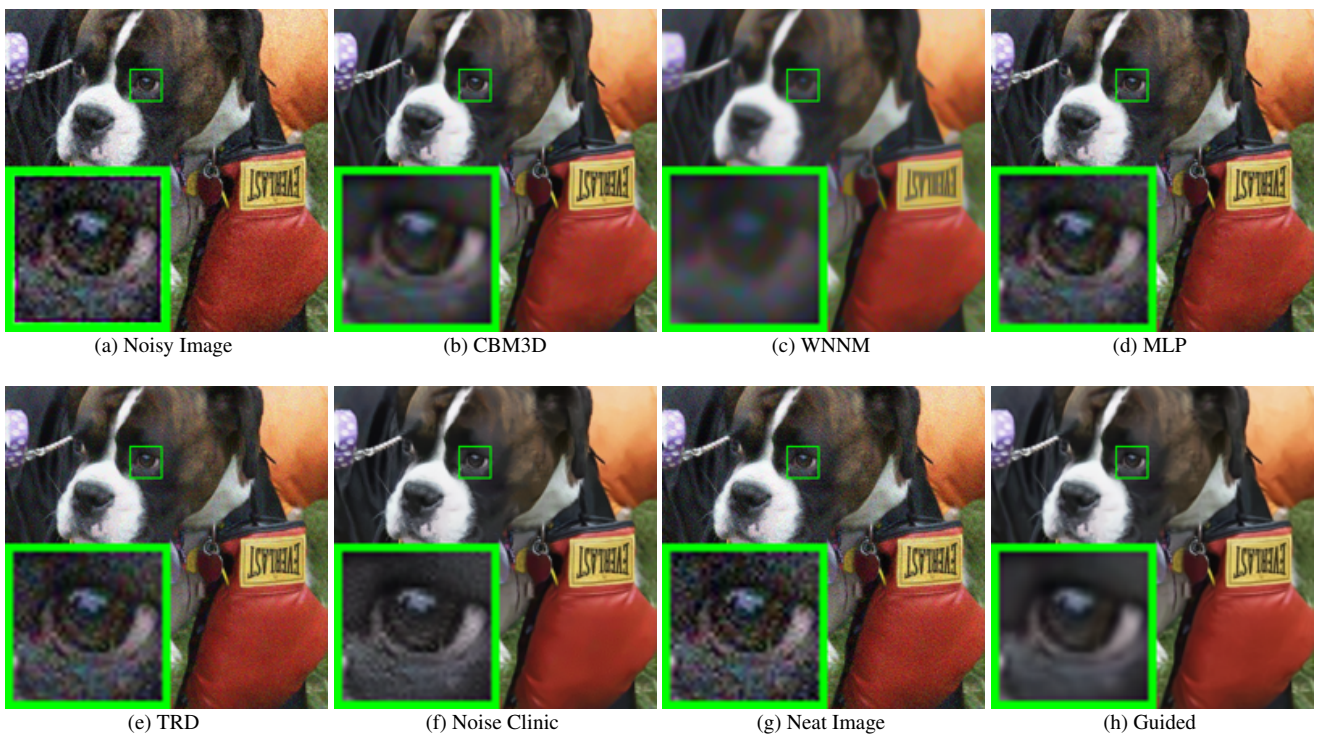


Figure 7. Denoised images of the image "5dmak3iso32003" by different methods. The images are better to be zoomed in on screen.

restoration. *Multiscale Modeling & Simulation*, 4(2):460–489, 2005. 5

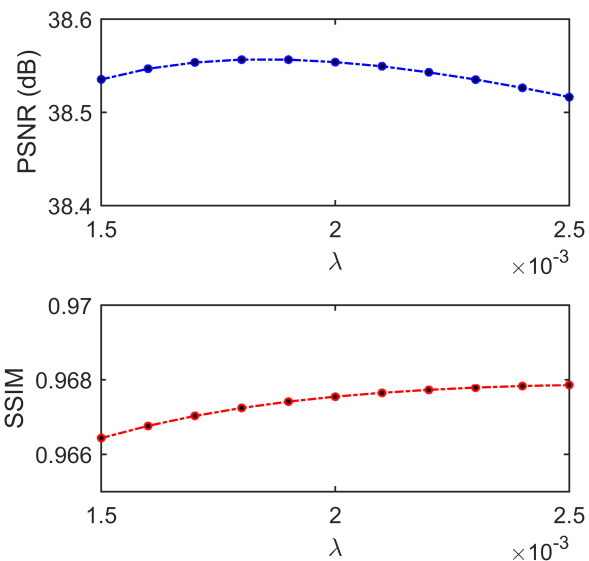


Figure 8. The PSNR/SSIM results as a function of the parameter  $\lambda$ .